

MM-GTUNets: Unified Multi-Modal Graph Deep Learning for Brain Disorders Prediction

Luhui Cai¹, Weiming Zeng¹, *Senior Member, IEEE*, Hongyu Chen¹, Hua Zhang¹,
Yueyang Li¹, Yu Feng¹, Hongjie Yan¹, Lingbin Bian¹, and Nizhuan Wang¹

Abstract—Graph deep learning (GDL) has demonstrated impressive performance in predicting population-based brain disorders (BDs) through the integration of both imaging and non-imaging data. However, the effectiveness of GDL based methods heavily depends on the quality of modeling the multi-modal population graphs and tends to degrade as the graph scale increases. Furthermore, these methods often constrain interactions between imaging and non-imaging data to node-edge interactions within the graph, overlooking complex inter-modal correlations, leading to suboptimal outcomes. To overcome these challenges, we propose MM-GTUNets, an end-to-end graph transformer based multi-modal graph deep learning (MMGDL) framework designed for brain disorders prediction at large scale. Specifically, to effectively leverage rich multi-modal information related to diseases, we introduce **Modality Reward Representation Learning (MRRL)** which adaptively constructs population graphs using a reward system. Additionally, we employ variational autoencoder to reconstruct latent representations of non-imaging features aligned with imaging features. Based on this, we propose **Adaptive Cross-Modal Graph Learning (ACMGL)**, which captures critical modality-specific and modality-shared features through a unified GTUNet encoder taking advantages of Graph UNet and Graph Transformer, and feature fusion module. We validated our method on two public multi-modal datasets ABIDE and ADHD-200, demonstrating its superior performance in diagnosing BDs. Our code is available at <https://github.com/NZWANG/MM-GTUNets>.

Index Terms—Graph deep learning, reward system, cross-modal learning, disease prediction.

I. INTRODUCTION

BRAIN disorders (BDs) such as Autism Spectrum Disorder (ASD), Attention Deficit Hyperactivity Disorder (ADHD), and others [1], [2] often exhibit complex pathological mechanisms and diverse clinical manifestations. These

BDs severely impact patients’ quality of life and social functioning. By 2021, over 3 billion individuals globally had been affected by different BDs, posing substantial challenges to the worldwide healthcare systems [3]. Currently, many clinical diagnoses of BDs are based on multi-modal medical data. However, the heterogeneous medical data makes it challenging for healthcare professionals to provide accurate and reliable diagnoses results in a timely manner [4].

The development of novel Artificial Intelligence (AI) prediction models is capable of processing large-scale multi-modal medical data for the clinical diagnosis of BDs [5]–[7]. For instance, [8], [9] used sparse dictionary learning to obtain the complementary features across modalities. The studies of [10], [11] introduced deep encoders tailored to different modalities to learn shared representations. However, these methods only focused on the complementarity and consistency in multi-modal data [12], and overlooked the correlation between subject populations which is crucial for diagnosing BDs [13]–[16].

Graph Deep Learning (GDL) [16], [17] gives a new perspective of predicting population-based BDs via integrating multi-modal information and uncovering relationships between different participants. Specifically, the graph-based models update the nodal features by aggregating the features of local neighborhoods of that node [18], [19]. The strategies of constructing population graphs include static graph construction and adaptive graph construction [20]. [13], [15] employed predefined similarity measures to assess the correlations between subjects’ multimodal features. These methods rely on manually designed similarity measures to construct the graph, which cannot be adjusted dynamically during training, resulting in poor generalization performance. [14], [21] designed a pairwise association encoder to dynamically adjust the edge weights of the population graph during training. Additionally, [22] examined the impact of various categories of non-imaging features on edge characteristics. They introduced an attention mechanism to compute affinity scores for non-imaging features and assign corresponding attention weights, which enhanced the capture of relational information between features.

One of the most popular and effective methods in GDL is Graph Neural Networks (GNNs) which has been widely applied in population-based BDs prediction [13], [17], [21]. Apart from GNNs, some studies have proposed Graph transformer (GT) to better address the complexity of population graphs [23], [24]. GT employed a self-attention mechanism to dynamically learn relationships between nodes. Self-attention

This work was supported by the National Natural Science Foundation of China [grant number 31870979]. (Corresponding author: Weiming Zeng, and Nizhuan Wang)

Luhui Cai, Weiming Zeng, Hongyu Chen, Hua Zhang, Yueyang Li and Yu Feng are with the Laboratory of Digital Image and Intelligent Computation, Shanghai Maritime University, Shanghai 201306, China (e-mail: clh0x123@126.com, zengwm86@163.com, hongychen676@gmail.com, zhanghua_hhz@163.com, lyy20010615@163.com, and fyuchn@163.com.)

Hongjie Yan is with the Department of Neurology, Affiliated Lianyungang Hospital of Xuzhou Medical University, Lianyungang 222002, China (email: yanhjns@gmail.com).

Lingbin Bian is with the School of Biomedical Engineering & State Key Laboratory of Advanced Medical Materials and Devices, ShanghaiTech University, Shanghai 201210, China (email: bianlb@shanghaitech.edu.cn)

Nizhuan Wang is with the Department of Chinese and Bilingual Studies, The Hong Kong Polytechnic University, Hong Kong, SAR, China (e-mail: wangnizhuan1120@gmail.com).

is suitable to the graphs of various shapes and sizes and dynamic node interactions, thereby captures better information within the graph structure. To date, numerous GT-based model architectures have been applied in BDs prediction research [25], [26].

Although the aforementioned methods have shown strong performance in population-based BDs prediction tasks, the challenges remain due to the diversity and complexity of multi-modal data between different individuals.

A. Underutilization of non-imaging Data

Using both Non-imaging data (e.g., gender, age, acquisition site, etc.) and imaging data (e.g. the resting-state functional magnetic resonance imaging (rs-fMRI)) [27], [28] can provide complementary information with each other. Integrating Non-imaging and imaging data helps to understand the manifestations of BDs. However, in the majority of previous studies, non-imaging data were only used for calculating affinity scores of the population graph and were not included as part of the subject features in the node embedding update process [13]–[15] in the GNN framework. This may result in underutilization of crucial information of non-imaging data. For this issue, [16], [29] attempted to construct parallel graphs for imaging and non-imaging data. However, due to significant modality differences between non-imaging and imaging data, merely incorporating low-dimensional non-imaging features as node embeddings cannot fully exploit their latent information. Although [22] has incorporated an attention mechanism into the model for initial exploration, the problem that each type of non-imaging data may influence the edge weights of the population graph differently still can not be solved.

B. Overlooking Crucial Node Features

The GNN is highly sensitive to the graph topology [18], [30]. In order to enhance the performance of GNN, we need to minimize the impact of noise when constructing population graphs. Most handcrafted graph construction methods [13], [15] and adaptive ones [14], [29] operate on large graphs which contain large number of subject nodes. However, these methods often do not fully consider the key features of nodes in the graph, instead process the entire graph uniformly, resulting in less attention to important nodes. A more effective approach involves introducing pooling layers to filter nodes and edges in the graph [19]. This approach has been applied in a previous BDs prediction study by [31], but its application in population-based BDs prediction has not been explored.

C. Insufficient Depth in Cross-Modal Interaction

In BDs diagnoses, imaging data reveals the changes of brain patterns, while non-imaging data reflects clinical and physiological characteristics. Cross-modal interaction which involves the exchange of information between these data types, is crucial for comprehensive patient assessment and effective diagnostic strategies. However, current approaches to cross-modal interaction between imaging and non-imaging data have some limitations. For instance, [13], [14] involve

cross-modal interaction only between nodes and edges in the graph, while [16], [25] merely fuse imaging and non-imaging features. These methods lack efficient interaction and fusion of different modal data, because of which the models may fail to completely exploit the complementary and consistent information of the imaging and non-imaging data.

To address the aforementioned issues, we proposed a multi-modal graph Deep Learning (MMGDL) framework for BDs prediction called MM-GTUNets: a unified encoder-decoder-based multi-modal graph learning framework, which is effective to encode the large-scale multi-modal data. The main contributions of this framework are as follows:

- We propose Modality-Rewarding Representation Learning (MRRL) for constructing an adaptive rewarding population graph. This process generates latent representations of non-imaging features and accurately analyzes their contribution weights through a meticulously designed affinity metric reward system (AMRS), thereby adaptively learning the population graph.
- We propose Adaptive Cross-Modal Graph Learning (ACMGL) for handling interactive learning between multi-modal data and capture complex inter- and intra-modal relationships. Moreover, the Graph TransUNet (GTUNet) can filter important node features through node down-sampling and effectively extract both global and local information, making it suitable for efficiently processing complex, large-scale graph data.
- We visualize the inter- and intra-modal contribution weights learned by the model, providing modality-interpretable decision support in medical applications.

The remainder of the paper is organized as follows: Sec. II reviews some work related to multi-modal graph deep learning. Sec. III elaborate the architecture of MM-GTUNets. Sec. IV describes the datasets and the implementation of results. Finally, Sec. V draws a conclusion and indicates future research direction.

II. RELATED WORK

A. Graph Deep Learning

Convolutional Neural Networks (CNNs) is capable of capturing multi-scale local features and constructing high-order representations [32]. However, CNNs are only suitable for Euclidean data (e.g., images and texts) and face limitations when dealing with non-Euclidean data (e.g., social or brain networks) [30]. To handle graph data, GNNs were proposed to deal with graph-related tasks [18], [23], [24]. Generally, GNNs-based BDs diagnoses methods can be categorized into brain graphs-based and population graphs-based ones [20], [33].

1) *Brain Graphs*: The human brain network can be modelled as a graph, where each region of interest (ROI) is a node, and the functional connectivity (FC) between a pair of ROIs is the edge weight. For instance, Brain-GNN uses an ROI-aware graph convolution layer and an ROI selection pooling layer to analyze brain networks for predicting neurobiomarkers at both group and individual levels [31]. To capture brain

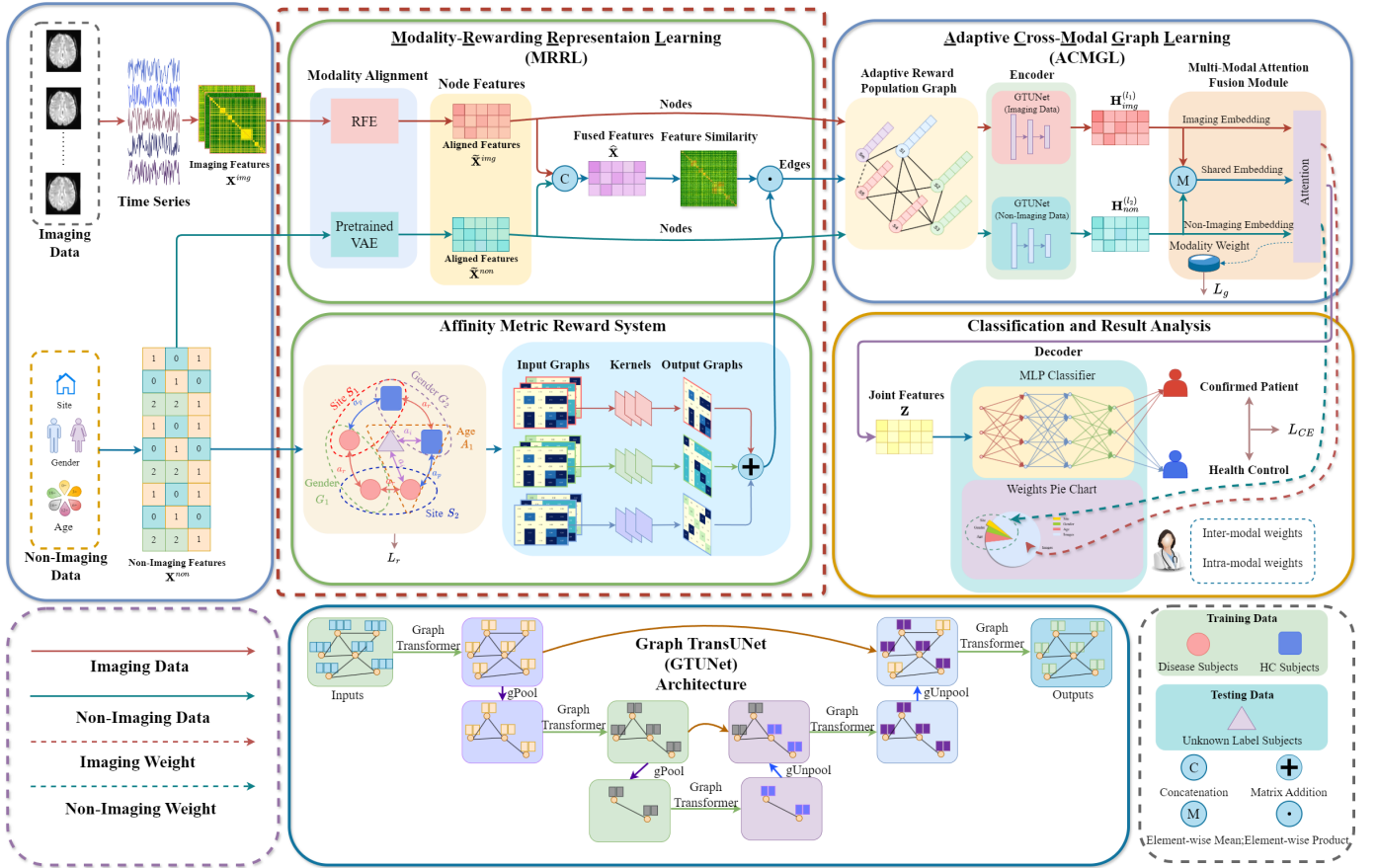


Fig. 1. The proposed MM-GTUNets framework for BDs prediction. In this paper, imaging data and non-imaging data refer to rs-fMRI and clinical data respectively.

connectome representations more efficiently, [34] proposed a dynamic graph convolution method and a convolutional pooling strategy for comprehensive graph information extraction. [35] introduced graph contrastive learning to FC matrix feature extraction to identify key functional connections and brain regions associated with BDs.

2) *Population Graphs*: In population graphs, each subject can be modelled as a node, with edge weights representing the association degree between subjects, by which each subject's feature representation can be processed on a single graph, providing higher efficiency and scalability compared to brain graph-based methods when handling large datasets [13]. To address the challenge of label collection in clinical diagnosis, [36] proposed a self-supervised learning framework based on dynamic FC analysis. Further, [21], [37] tackled the interpretability and biomarker detection issues in population graph modeling by proposing a hierarchical graph framework that considers both brain network topology and subject relationships.

B. Multi-Modal Graph Deep Learning

Multi-modal graph deep learning (MMGDL) has been widely applied in fields such as computer vision and natural language processing [38]. By integrating multi-modal data, MMGDL is able to decode more accurate and comprehensive information for BDs prediction. Based on [13], [14], a

modality-aware representation learning method for MMGDL was proposed by [29]. [39] designed an MMGDL architecture that employs multi-modal fusion strategy. Both approaches aimed to capture inter- and intra-modal relationships. Furthermore, studies by [22], [40] conducted brain network connectomics analysis on multi-modal imaging data to reveal the structure and dynamic changes of the brain functional networks, for biomarker identification and BDs diagnoses.

III. METHODOLOGY

A. Problem Formulation

1) *Overview of the Framework*: Our proposed end-to-end MM-GTUNets framework (Fig. 1) consists of three stages:

- **Modality-Rewarding Representation Learning**. MRRL is designed to accurately construct the population graph's adjacency matrix \mathbf{A} by aligning imaging features \mathbf{X}^{img} and non-imaging features \mathbf{X}^{non} . Specifically, its reward metric system can adaptively capture the significance of each type of non-imaging data.
- **Adaptive Cross-Modal Graph Learning**. Based on the modality-aligned features $\tilde{\mathbf{X}}$ and the adjacency matrix \mathbf{A} , the proposed unified encoder GTUNet and multi-modal attention module can achieve modality-joint representation \mathbf{Z} , consisting of modality-shared information and modality-specified information.

- **Classification Analysis.** This module uses a multi-layer perceptron (MLP) as an decoder to predict \hat{y} from \mathbf{Z} . Also, the contribution weights of each modality in prediction are visualized.

2) *Notation Definition:* Let $\mathbf{X} = [\mathbf{X}_1, \mathbf{X}_2 \cdots, \mathbf{X}_N]$ be the multi-modal features of N subjects, and $\mathbf{y} = [y_1, y_2, \cdots, y_N]$ is the corresponding labels. For a subject i with imaging and non-imaging features, we have $\mathbf{X}_i = [\mathbf{x}_i^{img}, \mathbf{x}_i^{non}]$. Also, subject i can be considered as node v_i , with its features represented as \mathbf{X}_i . Thus, the node set can be represented as $\mathcal{V} = \{v_i^{img}, v_i^{non}\}_{i=1}^N$. Further, the association strength between subject i and subject j is represented by the edge set $\mathcal{E} = \{e_{ij}\}_{i,j=1}^N$. Therefore, the population graph is represented by $\mathcal{G} = (\mathcal{V}, \mathcal{E}, \mathbf{X})$, with its adjacency matrix $\mathbf{A} \in \mathbb{R}^{N \times N}$ showing the edge weights as e_{ij} .

B. Modality-Rewarding Representation Learning

1) *Modality Alignment:* To ensure effectiveness of multi-modal features within two channels of our proposed framework, we conducted comprehensive feature processing for both imaging and non-imaging data.

For the given imaging features $\mathbf{x}_i^{img} \in \mathbb{R}^{d_1}$ of subject i , we use the recursive feature elimination (RFE) dimensional-reduction strategy [13] to convert into a relatively low-dimensional feature vector $\tilde{\mathbf{x}}_i^{img} \in \mathbb{R}^d$.

The low-dimensional non-imaging features $\mathbf{x}_i^{non} \in \mathbb{R}^{d_2}$ of subject i have modal gap with the high-dimensional imaging features. To mitigate the modal gap between non-imaging and imaging data, inspired by [41] on multimodal data imputation, we employed a pre-trained variational autoencoder (VAE) [42] to reconstruct the latent representation of \mathbf{x}_i^{non} , resulting in a relatively high-dimensional vector $\tilde{\mathbf{x}}_i^{non} \in \mathbb{R}^d$.

2) *Affinity Metric Reward System:* Q-Learning is a classic reinforcement learning approach that enables an agent to learn the optimal policy by interacting with the environment, adjusting actions, and updating the Q-table [43]. It can be used to model the contribution weight ratios of various types of non-imaging data in AMRS (Fig. 2). For each pairwise comparison of subjects, their non-imaging information (state) and labels (action) are transmitted to MRRL (agent). Then, the agent selects the optimal operation according to the value, allowing specific non-imaging data to have greater weight. The value is calculated based on the maintained three tables (i.e., reward, penalty, and motivation tables). By interacting with the subject population and their non-imaging data as the environment through the MRRL module, the AMRS learns the corresponding attention coefficients for each type of non-imaging data.

For convenience, we first give some mathematical notations in AMRS. The weights of the v types of non-imaging data are defined as α :

$$\alpha = [\alpha_1, \alpha_2, \cdots, \alpha_v],$$

$$s.t. \begin{cases} 0 < \alpha_1, \alpha_2, \cdots, \alpha_v < 1, \\ \sum_{u=1}^v \alpha_u = 1. \end{cases} \quad (1)$$

The reward, penalty, and motivation tables maintained by the agent are denoted as $\mathbf{R}, \mathbf{P}, \mathbf{M} \in \mathbb{R}^{N \times N}$, respectively.

Also, the corresponding weight coefficients corresponding to v types of non-imaging data are denoted as β :

$$\beta = \{\beta_r^u, \beta_p^u, \beta_m^u\}_{u=1}^v,$$

$$s.t. \begin{cases} \beta_r^u, \beta_m^u > 0, \beta_p^u < 0, \\ \beta_r^u + \beta_m^u < |\beta_p^u|. \end{cases} \quad (2)$$

Thus, the adjacency matrix of the non-imaging affinity graph can be defined as $\mathbf{C} \in \mathbb{R}^{N \times N}$, where C_{ij} between subject i and subject j through AMRS is calculated as follow:

$$C_{ij} = \text{Sigmoid} \left(\sum_{u=1}^v \alpha_u (\beta_r^u R_{ij} + \beta_p^u P_{ij} + \beta_m^u M_{ij}) \right). \quad (3)$$

Meanwhile, the R_{ij} , P_{ij} and M_{ij} are defined as:

$$\Phi_{ij} = \sum_{u=1}^v \phi_u(u_i, u_j), \quad (4)$$

where $(\Phi_{ij}, \phi_u) \in \{(R_{ij}, r_u), (P_{ij}, p_u), (M_{ij}, m_u)\}$. Specifically, $\phi_u(u_i, u_j)$ in Eq. 4 can update the states of three tables after subjects i and j through interacting with the u -th non-imaging data according to Eq. 5.

$$r_u(u_i, u_j) = \begin{cases} 1, & \text{if } u_i = u_j \text{ and } y_i = y_j, \\ 0, & \text{otherwise,} \end{cases}$$

$$p_u(u_i, u_j) = \begin{cases} 1, & \text{if } u_i = u_j \text{ and } y_i \neq y_j, \\ 0, & \text{otherwise,} \end{cases} \quad (5)$$

$$m_u(u_i, u_j) = \begin{cases} 1, & \text{if } u_i = u_j \text{ and } \{y_i, y_j\} \in \text{testset}, \\ 0, & \text{otherwise.} \end{cases}$$

Finally, to adaptively determine the optimal weights α in Eq. 3 for each type of non-imaging data in constructing the affinity graph, a state-action value function $Q(s, a)$ is designed to maximize the overall value, which incorporates the policy π as follow:

$$Q_\pi(s, a) = \mathbb{E}_\pi [G_t | S_t = s, A_t = a]$$

$$= \frac{1}{N^2} \sum_{u=1}^v \operatorname{argmax}_{\alpha_u}$$

$$\sum_{i=1}^N \sum_{j=1}^N \alpha_u \operatorname{ReLU}(\beta_r^u R_{ij} + \beta_p^u P_{ij}), \quad (6)$$

where G_t , S_t , and A_t represent the cumulative returns, the weights of non-image features and the labels of the compared subjects from the beginning to the t -th comparison, respectively. Further, we can rewrite the optimization for the adjacency matrix \mathbf{C}^* of the non-imaging affinity graph as:

$$\mathbf{C}^* \Leftrightarrow \operatorname{argmax}_{\pi} Q_\pi(s, a). \quad (7)$$

3) *Population Graph Construction:* Many studies have asserted that the fusion of cross-modal data can enhance the representation ability and improve model's performance [22], [29], [39]. Given the imaging features $\tilde{\mathbf{X}}^{img} \in \mathbb{R}^{N \times d}$, non-imaging features $\tilde{\mathbf{X}}^{non} \in \mathbb{R}^{N \times d}$, and the adjacency matrix \mathbf{C} of non-imaging affinity graph, the adaptive reward population graph (ARPG) construction is proposed to integrate key features of different modalities through the following steps:

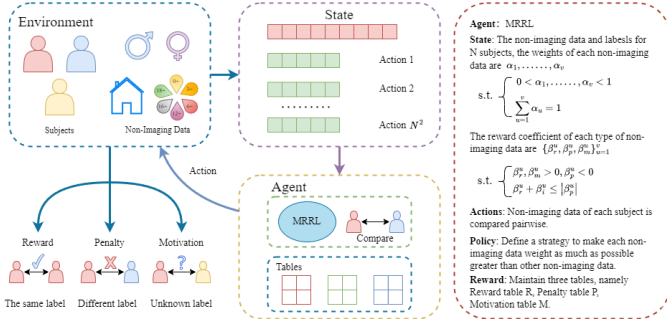


Fig. 2. Affinity Metric Reward System. AMRS adaptively adjusts the contribution weights of each type of non-imaging data and generates the non-imaging affinity graph, making the overall framework’s diagnostic process more intelligent.

- Step 1: Forming the node embeddings of ARPG by directly fusing the features from various modalities through $\hat{\mathbf{X}} = \text{Concat}(\hat{\mathbf{X}}^{img}, \hat{\mathbf{X}}^{non})$.
- Step 2: Generating the adjacency matrix \mathbf{A} of ARPG. $\hat{\mathbf{x}}_i$ denotes the fused feature vector of subject i . By integrating the non-imaging affinity graph \mathbf{C} and the subject similarity measurement from [13], each edge weight of the ARPG is computed as:

$$A_{ij} = \text{Sim}(\hat{\mathbf{x}}_i, \hat{\mathbf{x}}_j) \odot C_{ij}, \quad (8)$$

where \odot represents element-wise multiplication, and the similarity measurement $\text{Sim}(\cdot)$ is defined as follows:

$$\text{Sim}(\hat{\mathbf{x}}_i, \hat{\mathbf{x}}_j) = \exp\left(-\frac{[\rho(\hat{\mathbf{x}}_i, \hat{\mathbf{x}}_j)]^2}{2\sigma^2}\right), \quad (9)$$

where $\rho(\cdot)$ represents the correlation distance function, and σ denotes the width of the kernel.

In addition, inspired by the methodology [14], the Monte Carlo edge dropout strategy is involved in our framework to randomly remove edges during training such that the sparsity is induced. This strategy can mitigate over-smoothing and overfitting problems.

C. Adaptive Cross-Modal Graph Learning

1) *GTUNet Encoder:* In ACMGL module (Fig. 1), the GTUNet encoder is proposed to effectively extract modality-specific information from each modality channel, where the Graph Unets architecture [19] is used. The GT operation [44], [45] replaces the original graph convolution in the Graph Unets. The GTUNet includes the gPool layer for node downsampling, and the gUnpool layer for the corresponding inverse operation.

Firstly, given the constructed ARPG, the updating process of node features in GTUNet can be defined as a function $GTC(\cdot)$ through the GT layer, which can be concretely expressed as the following formulas. Let $\mathbf{H}^{(l)} = [\mathbf{h}_1^{(l)}, \mathbf{h}_2^{(l)}, \dots, \mathbf{h}_N^{(l)}]$ represent the l -th layer of node embeddings, where $\mathbf{H}^{(0)}$ equals the input features of the nodes $\tilde{\mathbf{X}} = [\tilde{\mathbf{X}}^{img}, \tilde{\mathbf{X}}^{non}]$ in ARPG.

The attention for each edge from node i to node j can be computed as:

$$\begin{aligned} \chi_i^{(l)} &= \mathbf{W}_\chi^{(l)} \mathbf{h}_i^{(l)} + \mathbf{b}_\chi^{(l)}, \text{ for } \chi \in \{\mathbf{q}, \mathbf{k}, \mathbf{v}\}, \\ \mathbf{e}_{ij} &= \mathbf{W}_e \mathbf{e}_{ij} + \mathbf{b}_e, \\ \alpha_{ij}^{(l)} &= \frac{\langle \mathbf{q}_i^{(l)}, \mathbf{k}_j^{(l)} + \mathbf{e}_{ij} \rangle}{\sum_{u \in \mathcal{N}(i)} \langle \mathbf{q}_i^{(l)}, \mathbf{k}_u^{(l)} + \mathbf{e}_{iu} \rangle}, \\ \bar{\mathbf{h}}_i^{(l+1)} &= \sum_{j \in \mathcal{N}(i)} \alpha_{ij}^{(l)} (\mathbf{v}_j^{(l)} + \mathbf{e}_{ij}), \end{aligned} \quad (10)$$

where $\mathcal{N}(i)$ denotes all the neighbors of node i , $\langle \mathbf{q}, \mathbf{k} \rangle = \exp\left(\frac{\mathbf{q}^T \mathbf{k}}{\sqrt{d}}\right)$ represents the scaled dot-product function, and d is the dimension of the attention hidden layer. To avoid the over-smoothing of the model, the gated residual connections are introduced as follow:

$$\begin{aligned} \mathbf{r}_i^{(l)} &= \mathbf{W}_r^{(l)} \mathbf{h}_i^{(l)} + \mathbf{b}_r^{(l)}, \\ \gamma_i^{(l)} &= \text{Sigmoid}\left(\mathbf{W}_g^{(l)} \left[\bar{\mathbf{h}}_i^{(l+1)}; \mathbf{r}_i^{(l)}; \bar{\mathbf{h}}_i^{(l+1)} - \mathbf{r}_i^{(l)}\right]\right), \\ \mathbf{h}_i^{(l+1)} &= \text{ReLU}\left(\text{LN}\left((1 - \gamma_i^{(l)}) \bar{\mathbf{h}}_i^{(l+1)} + \gamma_i^{(l)} \mathbf{r}_i^{(l)}\right)\right). \end{aligned} \quad (11)$$

Secondly, the downsampling and upsampling process of GTUNet will be elaborated based on ARPG. Let $\mathbf{A}^{(l)}$ denote the l -th layer adjacency matrix, with $\mathbf{A}^{(0)} = \mathbf{A}$. In terms of the downsampling processing of GTUNet, the node features $\mathbf{H}^{(l)}$ and adjacency matrix $\mathbf{A}^{(l)}$ are first fed into the gPool layer [19], followed by utilizing the top- k algorithm to select the \hat{k} nodes with the highest information and to output the filtered node features $\hat{\mathbf{H}}^{(l)}$ and adjacency matrix $\hat{\mathbf{A}}^{(l)}$ as follows:

$$\begin{aligned} \text{idx} &= \text{rank}(\delta, \hat{k}), \\ \hat{\mathbf{A}}^{(l)} &= \mathbf{A}^{(l)}(\text{idx}, \text{idx}), \\ \hat{\mathbf{H}}^{(l)} &= \mathbf{H}^{(l)}(\text{idx}, :) \odot (\text{Sigmoid}(\delta(\text{idx})) \mathbf{1}_{d_h}^T), \end{aligned} \quad (12)$$

where δ represents the projection of $\mathbf{H}^{(l)}$ on the learnable vector, \hat{k} represents the number of nodes selected in the new graph, $\text{rank}(\delta, \hat{k})$ is a node ranking operation that returns the indices of the \hat{k} largest values in δ , and idx denotes the indices selected in the new graph. $\mathbf{A}^{(l)}(\text{idx}, \text{idx})$ and $\mathbf{H}^{(l)}(\text{idx}, :)$ represent the row and column extraction to form the feature matrix $\hat{\mathbf{H}}^{(l)}$ and adjacency matrix $\hat{\mathbf{A}}^{(l)}$ as inputs to $GTC(\cdot)$. Notably, when l is 0, $\hat{\mathbf{H}}^{(0)} = \mathbf{H}^{(0)}$ and $\hat{\mathbf{A}}^{(0)} = \mathbf{A}^{(0)}$. $\delta(\text{idx})$ extracts the values of δ with indices idx and applies the $\text{Sigmoid}(\cdot)$ operation. $\mathbf{1}_{d_h}^T \in \mathbb{R}^{d_h}$ is a one-dimensional tensor of size d_h with all components having a value of 1, where d_h is the neuron number at the hidden layer. \odot denotes element-wise multiplication.

After the downsampling process which extracts important node features using l gPool layers, we also need to use l gUnpool layers to restore the graph to its original structure for subsequent classification tasks. Thus, the downsampling processing of GTUNet can be expressed by performing θ gUnpool layers:

$$\tilde{\mathbf{H}}^{(l+\theta)} = \text{Distribute}\left(\mathbf{H}^{(l-\theta)}, \mathbf{H}^{(l+\theta)}, \text{idx}^{(l-\theta)}\right), \quad (13)$$

where $\tilde{\mathbf{H}}^{(l+\theta)}$ represents the restored feature matrix after executing the gUnpool layer at the $(l + \theta)$ -th layer. Due to

the symmetry of GTUNet structure, the pre-filtered feature matrix and index are denoted as $\mathbf{H}^{(l-\theta)}$ and $\text{idx}^{(l-\theta)}$, with the corresponding adjacency matrix denoted as $\mathbf{A}^{(l-\theta)}$. The $\text{Distribute}(\cdot)$ operation distributes the row vectors from $\mathbf{H}^{(l+\theta)}$ to the feature matrix $\mathbf{H}^{(l-\theta)}$ according to the indices stored in $\text{idx}^{(l-\theta)}$.

Finally, after obtaining the feature matrix $\mathbf{H}^{(2l)}$ restored to its initial structure through l gUnpool layers, we perform additional $\text{GTC}(\cdot)$ operation. In GTUNet, a total of $2l + 1$ $\text{GTC}(\cdot)$ operations are performed, resulting in $2l + 1$ GT layers. For simplicity, we denote the overall process of GTUNet encoder as a function $\text{GTU}(\cdot)$.

2) *Multi-Modal Attention Fusion Module*: Inspired by [39], based on the outputs by GTUNet encoder for each modality, we propose a multi-modal attention fusion module to effectively achieve modality-joint representations that encompass both modality-specific and shared information, which can be formulated as follows:

$$\begin{aligned}\mathbf{Z}_{sp}^{img} &= \text{GTU}^{(l_1)}(\tilde{\mathbf{X}}^{img}), \\ \mathbf{Z}_{sp}^{non} &= \text{GTU}^{(l_2)}(\tilde{\mathbf{X}}^{non}), \\ \mathbf{Z}_{sh} &= \frac{1}{2}(\mathbf{Z}_{sp}^{img} + \mathbf{Z}_{sp}^{non}),\end{aligned}\quad (14)$$

where l represents the layers of the encoder, \mathbf{Z}_{sp}^{img} and \mathbf{Z}_{sp}^{non} are the modality-specific embeddings for the imaging and non-imaging features, respectively, and \mathbf{Z}_{sh} is the modality-shared embedding.

Next, the attention weights of the modality-shared embedding and two modality-specific embeddings can be expressed as:

$$\begin{aligned}\tau_{sh} &= \tanh(\mathbf{W}\mathbf{Z}_{sh} + \mathbf{B}), \\ \tau_{sp}^{img} &= \tanh(\mathbf{W}^{img}\mathbf{Z}_{sp}^{img} + \mathbf{B}^{img}), \\ \tau_{sp}^{non} &= \tanh(\mathbf{W}^{non}\mathbf{Z}_{sp}^{non} + \mathbf{B}^{non}),\end{aligned}\quad (15)$$

where \mathbf{W} , \mathbf{W}^{img} , and \mathbf{W}^{non} represent the weight matrices, while \mathbf{B} , \mathbf{B}^{img} , and \mathbf{B}^{non} denote the bias matrices.

After obtaining the attention weights, i.e., \mathbf{Z}_{sh} , \mathbf{Z}_{sp}^{img} and \mathbf{Z}_{sp}^{non} , the final embedding can be derived by combining these weights with the embeddings as below:

$$\mathbf{Z} = \tau_{sh} \odot \mathbf{Z}_{sh} + \tau_{sp}^{img} \odot \mathbf{Z}_{sp}^{img} + \tau_{sp}^{non} \odot \mathbf{Z}_{sp}^{non}, \quad (16)$$

where \odot signifies the element-wise multiplication, and \mathbf{Z} represents the joint representation of multi-modal features.

D. Classification and Result Analysis

For classification stage, the final prediction process can be achieved as $\hat{\mathbf{y}} = \text{MLP}(\mathbf{Z})$ based on the joint modality representation \mathbf{Z} .

Meanwhile, we compute the contribution weight scores for each modality based on the attention weights in Eq. 15 as:

$$\begin{aligned}\omega &= (\omega_{img}, \omega_{non}) \\ &= \text{Softmax}(f(\tau_{sp}^{img}, \tau_{sh}), f(\tau_{sp}^{non}, \tau_{sh})), \\ f(\cdot) &= \frac{\text{tr}(\boldsymbol{\tau}_{sp}, \boldsymbol{\tau}_{sp})}{\text{tr}(\boldsymbol{\tau}_{sh}, \boldsymbol{\tau}_{sh})},\end{aligned}\quad (17)$$

where ω_{img} and ω_{non} represent the weights for imaging features and non-imaging features, respectively.

E. Objective Function

The objective function for MM-GTUNets is as follows:

$$\mathcal{L}_{total} = \mathcal{L}_{ce} + \omega_{img}\mathcal{L}_g^{img} + \omega_{non}(\mathcal{L}_g^{non} + \eta\mathcal{L}_r), \quad (18)$$

where \mathcal{L}_{ce} , \mathcal{L}_g^{img} , and \mathcal{L}_g^{non} denotes the cross-entropy loss, and the graph regularization terms for imaging and non-imaging features, respectively; ω_{img} , ω_{non} are the learnable parameters, and η stands for the hyperparameter.

1) *Graph Regularization*: The structure of the graph significantly impacts the performance of GDL. In adaptive graph learning, fine-tuning the smoothness and sparsity emerges as a pivotal concern. Inspired by [29], we design the graph regularization as follows:

$$\begin{aligned}\mathcal{L}_g^\psi &= \lambda\mathcal{L}_{smh}^\psi + \mu\mathcal{L}_{deg}, \\ \mathcal{L}_{smh}^\psi &= \frac{1}{2N^2} \sum_{i,j=1}^N A_{ij} \|\mathbf{z}_i^\psi - \mathbf{z}_j^\psi\|_2^2, \\ \mathcal{L}_{deg} &= -\frac{1}{N} \mathbf{1}^T \log(\mathbf{A} \cdot \mathbf{1}),\end{aligned}\quad (19)$$

where $\psi \in \{img, non\}$, \mathcal{L}_{smh}^ψ , and \mathcal{L}_{deg} represent the smoothness regularization and the degree regularization of the graph along with the hyperparameters λ and μ .

2) *Reward Regularization*: In Sec. III-B, we optimized the non-imaging affinity graph \mathbf{C} using the designed state-action value function $Q_\pi(s, a)$. According to Eq. 7, optimizing \mathbf{C} is equivalent to maximizing $Q_\pi(s, a)$ via policy π . Thus, we can derive:

$$\begin{aligned}\text{argmin } \mathcal{L}_r &= \text{argmax } Q_\pi(s, a), \\ &= \text{argmin} \left(\frac{1}{Q_\pi(s, a)} \right).\end{aligned}\quad (20)$$

IV. EXPERIMENTAL RESULTS AND ANALYSIS

A. Datasets and Pre-Processing

Our proposed MM-GTUNets has been evaluated on two public brain imaging datasets: ABIDE and ADHD-200. The corresponding demographic information is detailed in Table I. In this study, we utilized rs-fMRI scans as the neuroimaging data. As a high proportion of fields are missing or invalid in the original data, we only include the subjects' gender, age and acquisition site as non-imaging data.

1) *ABIDE*: The Autism Brain Imaging Data Exchange (ABIDE) community [28] has compiled neuroimaging and non-imaging data from 20 different international acquisition sites. To ensure a fair comparison with previous state-of-the-art (SOTA) methods [13], [14], [29], we selected a cohort of 871 subjects from ABIDE, comprising 468 healthy controls (HC) and 403 ASD patients.

2) *ADHD-200*: The ADHD-200 dataset [28] includes rs-fMRI data and corresponding non-imaging data from 8 international acquisition sites. Following the methodology of [34], we chose data from four sites: New York University Medical Center, Peking University, Kennedy Krieger Institute, and the University of Pittsburgh. Due to the missing data in some samples, we ultimately included 582 subjects consisting of 364 HC and 218 ADHD patients.

3) *Pre-Processing*: For the rs-fMRI data from ABIDE and ADHD-200, preprocessing was conducted according to the C-PAC¹ [46] and Athena² [28] pipeline configurations, respectively. Using the Anatomical Automatic Labeling (AAL) brain atlas [47], we segmented the rs-fMRI data into 116 regions of interest (ROIs). For each ROI, we computed the average time series and then calculated the FC matrix for each subject using Pearson’s correlation coefficient. Finally, we extracted the upper triangular elements of each FC matrix and flattened them into a one-dimensional vector \mathbf{x}^{img} .

For the corresponding non-imaging data, the categorical data were encoded as one-hot form, while the numerical data were directly converted into float values. Then, these data were concatenated into a one-dimensional vector \mathbf{x}^{non} .

TABLE I
DEMOGRAPHIC STATISTICS OF THE DATASETS USED IN THIS WORK

Dataset	Diagnosis	Subject	Gender	Age
			(Female / Male)	(Mean \pm Std.)
ABIDE	HC	468	90 / 378	16.84 \pm 7.23
	ASD	403	54 / 349	17.07 \pm 7.95
ADHD-200	HC	364	166 / 198	12.42 \pm 8.62
	ADHD	218	39 / 179	11.56 \pm 5.91

B. Implementation Details

Our MM-GTUNets runs on a server equipped with 12 NVIDIA GeForce 4090 GPUs and is deployed on the PyTorch with Adam optimizer [48], with a total of 1.19M trainable parameters. For the initial pre-training of the VAE, we set the learning rate to be 1e-3, the weight decay rate to be 5e-4, and the model is trained for 3000 epochs. After freezing the pre-trained VAE, we optimized all model parameters with a learning rate of 1e-4 and a weight decay rate of 5e-4 over 500 epochs, using a dropout rate and edge dropout rate of 0.3. Early stopping with a patience of 100 epochs was employed to prevent overfitting.

During feature alignment, the dimensions of imaging and non-imaging features are downsampled or upsampled to 500 dimensions, respectively. The GTUNets encoder depths for imaging and non-imaging features are set to 2 and 3, respectively, with a graph pooling ratio of 0.8. For the ABIDE dataset, the hyperparameters λ , μ , and η in Eqs. 18 and 19 are set to 1, 1e-4, and 1e-2, respectively. For the ADHD-200 dataset, these hyperparameters are set to 1, 1e-1, and 1e-2, respectively.

C. Competitive Methods

1) *Performance Evaluation*: We evaluated the performance of the proposed method on the ABIDE (HC vs. ASD) and ADHD-200 (HC vs. ADHD) datasets using 10-fold stratified cross-validation. In each fold, the dataset is rotated so that each subset serves as the test set once, while the remaining nine

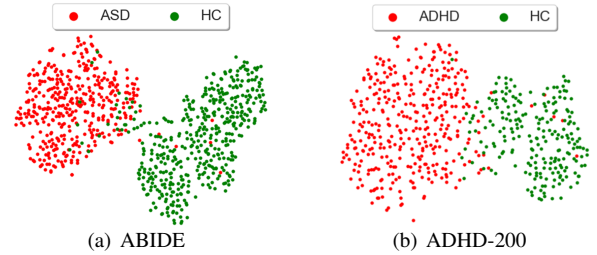


Fig. 3. Visualization of the joint representation of modalities.

fold are split into training and validation sets in a 9:1 ratio. The performance evaluation metrics, i.e., accuracy (ACC), sensitivity (SEN), specificity (SPE) and area under the ROC curve (AUC), are reported as the average of the 10-fold results on test datasets.

2) *Baselines*: We compared the proposed MM-GTUNets with a few traditional machine learning methods and several SOTA methods in disease prediction tasks. The traditional machine learning methods include support vector machine (SVM) and MLP, where the FC matrix was extracted as a one-dimensional vector and used as input after dimensionality reduction using RFE. The competing SOTA methods include Brain-GNN [31], DGCN [34], AL-NEGAT [40], A-GCL [35], Pop-GCN [13], GATE [36], EV-GCN [14], and MMGL [29].

3) *Qualitative Results*: Table II reports the quantitative performance of MM-GTUNets, where the prefixes “(T)”, “(B)”, and “(P)” denote traditional machine learning methods, brain-graph-based methods, and population-graph-based methods, respectively. Based on Table II, we can see that: (i) Compared to brain-graph-based methods, population-graph-based methods exhibit more stable performance, with smaller standard deviations in performance metrics. This stability may result from brain-graph methods focusing on local brain region features for each subject, while population-graph methods emphasize global association features within the subject population [33]. (ii) Most multi-modal methods outperform single-modal ones by integrating multiple data sources. Each modality provides unique information, enabling the model to capture a broader range of details. (iii) MM-GTUNets demonstrated outstanding performance on both datasets. For the ABIDE dataset, MM-GTUNets outperformed all comparison baselines across all metrics. For the ADHD-200 dataset, MM-GTUNets achieved the best results in all metrics except sensitivity and specificity.

4) *Visualization of Modality-Joint Representation*: To assess the capability of MM-GTUNets in learning cross-modality interactions, we utilized t-SNE [49] to visualize the modality-joint representation \mathbf{Z} in a two-dimensional space for the ABIDE and ADHD-200 datasets. As shown in Fig. 3, \mathbf{Z} forms two distinct clusters corresponding to the categories, indicating that the multi-modal features learned by MM-GTUNets exhibit significant discriminative power, with low intra-class and high inter-class dispersion.

D. Ablation Studies

1) *Effectiveness of Non-imaging Feature Reconstructor*: To assess the effectiveness of the proposed non-imaging feature

¹<https://github.com/preprocessed-connectomes-project/abide>

²<https://www.nitrc.org/plugins/mwiki/index.php/neurobureau:AthenaPipeline>

TABLE II
PERFORMANCE COMPARISON OF DIFFERENT METHODS ON ABIDE AND ADHD-200 DATASETS. "MM" INDICATES MULTI-MODAL DATA USAGE: "×" FOR SINGLE-MODAL, "✓" FOR MULTI-MODAL. (BOLD: OPTIMAL, UNDERLINE: SUBOPTIMAL)

Method	MM	ABIDE				ADHD-200			
		HC vs. ASD				HC vs. ADHD			
		ACC (%)	SEN (%)	SPE (%)	AUC (%)	ACC (%)	SEN (%)	SPE (%)	AUC (%)
(T)SVM	×	66.02 (0.35)	65.34 (0.26)	78.83 (0.43)	64.97 (0.37)	66.48 (0.16)	64.56 (2.16)	22.04 (0.62)	57.59 (0.21)
(T)MLP	×	72.69 (0.84)	72.02 (2.84)	73.45 (0.61)	77.69 (1.02)	75.28 (0.33)	62.81 (3.59)	82.64 (0.47)	82.03 (0.40)
(B)Brain-GNN [31]	×	69.76 (3.80)	67.47 (3.10)	73.28 (3.26)	72.50 (3.10)	65.26 (3.60)	68.59 (3.30)	63.05 (4.00)	66.02 (5.50)
(B)DGCN [34]	×	71.83 (2.90)	70.90 (2.59)	71.80 (3.10)	72.45 (2.98)	68.81 (3.69)	69.08 (4.07)	69.53 (4.71)	70.05 (4.57)
(B)AL-NEGAT [40]	✓	73.17 (3.32)	78.18 (2.66)	73.28 (3.14)	75.02 (2.56)	69.15 (3.82)	69.28 (4.32)	72.26 (3.92)	68.25 (3.69)
(B)A-GCL [35]	×	79.04 (2.40)	81.42 (3.03)	<u>80.95 (3.19)</u>	<u>82.86 (2.91)</u>	80.11 (4.30)	82.04 (4.58)	80.08 (4.10)	78.78 (4.39)
(P)Pop-GCN [13]	✓	68.43 (0.86)	78.32 (0.89)	57.51 (5.99)	73.90 (3.08)	75.45 (0.32)	50.99 (1.96)	<u>90.11 (0.22)</u>	81.72 (1.40)
(P)GATE [36]	×	74.65 (2.50)	75.59 (2.43)	76.87 (2.27)	76.87 (2.27)	72.20 (0.23)	77.27 (5.20)	72.40 (3.78)	74.61 (3.30)
(P)EV-GCN [14]	✓	<u>80.95 (0.27)</u>	<u>83.74 (0.61)</u>	77.69 (0.18)	82.37 (0.29)	<u>80.95 (0.96)</u>	60.33 (7.64)	93.11 (0.13)	<u>87.15 (1.15)</u>
(P)MMGL [29]	✓	80.34 (0.18)	80.25 (0.21)	77.16 (3.15)	79.83 (1.06)	77.59 (3.64)	76.21 (2.98)	74.57 (1.25)	78.47 (2.29)
MM-GTUNets (Ours)	✓	82.92 (0.54)	84.22 (0.81)	81.43 (0.64)	88.21 (0.61)	82.68 (0.60)	<u>77.58 (2.11)</u>	85.76 (0.46)	90.71 (0.72)

TABLE III
ABLATION STUDY OF NON-IMAGING FEATURE RECONSTRUCTOR IN MM-GTUNETS.(BOLD:OPTIMAL, UNDERLINE:SUBOPTIMAL)

Reconstructor	ABIDE		ADHD-200	
	ACC (%)	AUC (%)	ACC (%)	AUC (%)
MRRL w/o VAE	67.06 (3.27)	69.99 (4.26)	76.47 (1.93)	83.72 (3.07)
MRRL + MLP	<u>80.86 (0.84)</u>	<u>87.26 (1.20)</u>	<u>79.04 (0.23)</u>	<u>89.95 (0.23)</u>
MRRL + AE	76.02 (1.59)	82.42 (2.08)	77.86 (0.37)	89.85 (0.36)
MRRL w/ VAE	82.92 (0.54)	88.21 (0.61)	82.68 (0.60)	90.71 (0.72)

TABLE IV
ABLATION STUDY OF THE ENCODER ARCHITECTURE IN MM-GTUNETS.(BOLD:OPTIMAL, UNDERLINE:SUBOPTIMAL)

Architecture	ABIDE		ADHD-200	
	ACC (%)	AUC (%)	ACC (%)	AUC (%)
Stacked GTC	77.06 (0.47)	84.03 (0.71)	76.14 (0.61)	86.21 (0.81)
Residual GTC	78.78 (0.61)	85.56 (0.79)	76.33 (0.69)	88.26 (0.58)
Cascade GTC	<u>79.70 (0.47)</u>	<u>86.78 (0.57)</u>	<u>80.97 (0.54)</u>	<u>89.37 (0.61)</u>
GTUNet	82.92 (0.54)	88.21 (0.61)	82.68 (0.60)	90.71 (0.72)

reconstructor in MMRL (Sec. III-B), we compared the performance of different reconstruction methods (VAE, MLP, and autoencoder(AE)) across two datasets. As shown in Table III, the MMRL module performs poorly without the non-imaging feature reconstructor, while the VAE significantly outperforms the other two methods across both datasets.

2) *Effectiveness of Encoder Architecture*: To investigate the impact of encoder architectures on MM-GTUNets performance, we evaluated the GTC operator using stacked architecture, residual architecture, cascade architecture, and Graph Unets architecture. As shown in Table IV, among these four architectures, the GTUNet with the Graph Unets achieved the best performance, confirming the effectiveness of the GTUNet architecture introduced in Sec. III-C.

3) *Impact of Embedding Dimensions and Pooling Ratios*: To analyze the impact of embedding dimensions of multi-modal features on MM-GTUNets' performance, we tested a range of 250 to 2500 with step length equal to 250. As shown in Fig. 4(a), different from the findings in [13], [14], [36], on both datasets, the performance of MM-GTUNets peaked at an

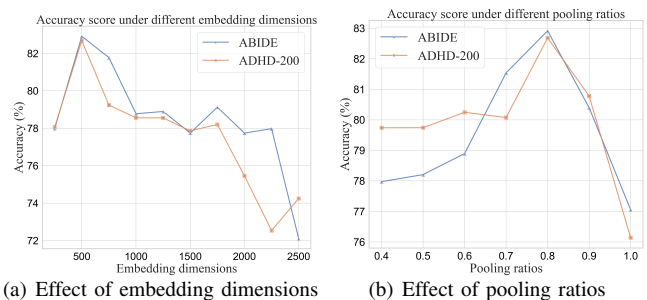


Fig. 4. Accuracy of MM-GTUNets with different embedding dimensions and different pooling ratios.

embedding dimension of 500 and then gradually declined. This decline may result from excessively high embedding dimensions causing redundant multi-modal feature representations, which degrades the performance.

To reveal the impact of the graph pooling ratios of the multi-modal data encoder GTU, we tested a range of 0.4 to 1.0 with step length equal to 0.1. Similarly, as shown in Fig. 4(b), in both datasets, the performance of MM-GTUNets peaked at a pooling ratio of 0.8 and then gradually declined, reaching its lowest point at a pooling ratio of 1.0. Low pooling ratios may remove important node features and edges, causing the loss of critical information, while high pooling ratios may neglect key features and significantly reduce the performance.

4) *Effectiveness of MRRL*: To evaluate the effectiveness of the adaptive reward-based population graph construction, we compared our MRRL method with other population graph construction methods, i.e., Pop-Graph (static) [13], EV-Graph (adaptive) [14], and MCA-Graph (adaptive) [22]. In this ablation study, we replaced the AMRS in the MRRL module with the non-imaging affinity calculation methods from Pop-Graph, EV-Graph, and MCA-Graph, respectively. As shown in Fig. 5, the manually constructed Pop-Graph performs the worst among all methods. Compared to adaptive graph construction baselines like EV-Graph and MCA-Graph, our MRRL shows overall better performance.

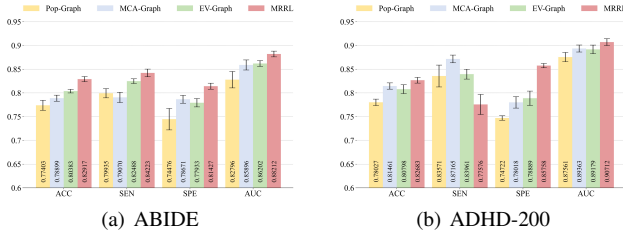


Fig. 5. Ablation study of graph construction methods in MM-GTUNets.

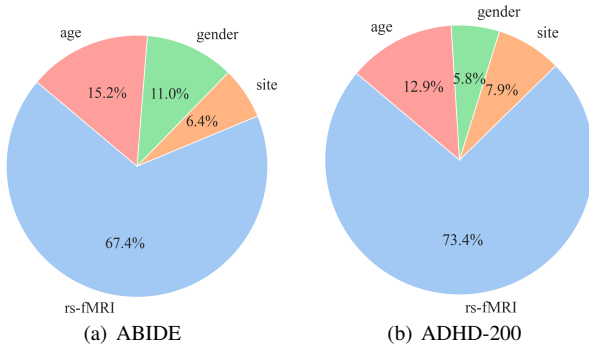


Fig. 6. The contribution weight of each modality for classification tasks.

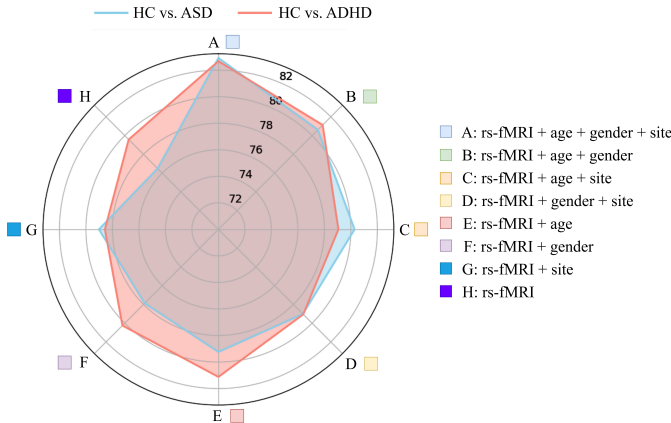


Fig. 7. The effect of each modality on the classification accuracy on ABIDE and ADHD-200.

E. Interpretability Analysis

To quantify each modality’s contribution in prediction tasks, we calculated the contribution weights for each modality, including various non-imaging data. As shown in Fig. 6, the average contribution weights on two datasets using MM-GTUNets reveal that rs-fMRI data contributes the most to predictions. Among non-imaging data, age has the greatest impact on prediction results.

According to Fig. 7, the model incorporating rs-fMRI and all non-imaging data types achieves the highest accuracy on both datasets. Among models containing only a single type of non-imaging data, the models containing age perform best. Thus, on ABIDE and ADHD-200, our MM-GTUNets effectively capture complex inter- and intra-modality relationships.

V. DISCUSSION AND CONCLUSION

In this paper, we propose a unified multi-modal graph deep learning framework named MM-GTUNets for BDs prediction based on the graph transformer to capture complex inter- and intra- modal relationships within large-scale multi-modal data. Importantly, the proposed affinity metric reward system helps adaptively learn the population graph and considers the contribution weights of non-imaging features. Furthermore, we propose the GTUNet to extract critical local node embedding from the global context within the graph, which incorporates the advantages of Graph Unets architecture and graph transformer operation. Finally, the modality-joint representation is formed by the embedding of different modalities through the feature fusion module. The module can also provide the visualization of the inter- and intra-modal contribution weights learned by the model, which makes our framework have the potential to bring modality-interpretable decision support in medical applications.

There are some avenues for future work. For example, despite MM-GTUNets has demonstrated satisfactory performance in binary classification tasks using rs-fMRI data and non-imaging data, studies on multi-classification tasks using more modalities (e.g., TADPOLE dataset [50]) could be further explored. Moreover, most existing multi-modal approaches only learn from samples with complete modalities, leaving much data underutilized. Extending our work to incomplete multi-modal learning [51], [52] tasks would be valuable. Considering that the medical personnel often need to make real-time or quick decisions in clinical settings, our framework based on transductive learning may not be suitable for real-time applications due to the need of processing additional test data during prediction. In future work, we will adapt MM-GTUNets to support inductive learning scenarios as described in [17], [29].

REFERENCES

- [1] T. Hirota and B. H. King, “Autism Spectrum Disorder: A Review,” *JAMA*, vol. 329, no. 2, p. 157, 2023.
- [2] J. Posner, G. V. Polanczyk, and E. Sonuga-Barke, “Attention-deficit hyperactivity disorder,” *The Lancet*, vol. 395, no. 10222, pp. 450–462, 2020.
- [3] J. D. Steinmetz, K. M. Seeher, N. Schiess, E. Nichols, B. Cao, C. Servili *et al.*, “Global, regional, and national burden of disorders affecting the nervous system, 1990–2021: A systematic analysis for the Global Burden of Disease Study 2021,” *The Lancet Neurology*, vol. 23, no. 4, pp. 344–381, 2024.
- [4] J. Yanase and E. Triantaphyllou, “A systematic survey of computer-aided diagnosis in medicine: Past and present developments,” *Expert Syst. Appl.*, vol. 138, p. 112821, 2019.
- [5] J. N. Acosta, G. J. Falcone, P. Rajpurkar, and E. J. Topol, “Multimodal biomedical AI,” *Nat. Med.*, vol. 28, no. 9, pp. 1773–1784, 2022.
- [6] M. Salvi, H. W. Loh, S. Seoni, P. D. Barua, S. García, F. Molinari *et al.*, “Multi-modality approaches for medical support systems: A systematic review of the last decade,” *Inf. Fusion*, vol. 103, p. 102134, 2024.
- [7] K. Saab, T. Tu, W.-H. Weng, R. Tanno, D. Stutz, E. Wulczyn *et al.*, “Capabilities of Gemini Models in Medicine,” arXiv:2404.18416, 2024.
- [8] Y. Huang, L. Shao, and A. F. Frangi, “Cross-Modality Image Synthesis via Weakly Coupled and Geometry Co-Regularized Joint Dictionary Learning,” *IEEE Trans. Med. Imaging*, vol. 37, no. 3, pp. 815–827, 2018.
- [9] G. Wu, Y. Chen, Y. Wang, J. Yu, X. Lv, X. Ju *et al.*, “Sparse Representation-Based Radiomics for the Diagnosis of Brain Tumors,” *IEEE Trans. Med. Imaging*, vol. 37, no. 4, pp. 893–905, 2018.

- [10] H. Yang, J. Sun, and Z. Xu, "Learning unified hyper-network for multi-modal mr image synthesis and tumor segmentation with missing modalities," *IEEE Trans. Med. Imaging*, vol. 42, no. 12, pp. 3678–3689, 2023.
- [11] Q. Zhu, B. Xu, J. Huang, H. Wang, R. Xu, W. Shao *et al.*, "Deep Multi-Modal Discriminative and Interpretability Network for Alzheimer's Disease Diagnosis," *IEEE Trans. Med. Imaging*, vol. 42, no. 5, pp. 1472–1483, 2023.
- [12] C. Zhang, Z. Yang, X. He, and L. Deng, "Multimodal Intelligence: Representation Learning, Information Fusion, and Applications," *IEEE J. Sel. Top. Signal Process.*, vol. 14, no. 3, pp. 478–493, 2020.
- [13] S. Parisot, S. I. Ktena, E. Ferrante, M. Lee, R. Guerrero, B. Glocker *et al.*, "Disease prediction using graph convolutional networks: Application to Autism Spectrum Disorder and Alzheimer's disease," *Med. Image Anal.*, vol. 48, pp. 117–130, 2018.
- [14] Y. Huang and A. C. Chung, "Disease prediction with edge-variational graph convolutional networks," *Med. Image Anal.*, vol. 77, p. 102375, 2022.
- [15] A. Kazi, S. shekarforoush, S. A. krishna, H. Burwinkel, G. Vivar, K. Kortuem *et al.*, "InceptionGCN: Receptive Field Aware Graph Convolutional Network for Disease Prediction," arXiv:1903.04233, 2019.
- [16] L. Cosmo, A. Kazi, S.-A. Ahmadi, N. Navab, and M. Bronstein, "Latent-graph learning for disease prediction," arXiv:2003.13620, 2020.
- [17] A. Kazi, L. Cosmo, S.-A. Ahmadi, N. Navab, and M. M. Bronstein, "Differentiable graph module (dgm) for graph convolutional networks," *IEEE Trans. Pattern Anal. Mach. Intell.*, vol. 45, no. 2, pp. 1606–1617, 2022.
- [18] T. N. Kipf and M. Welling, "Semi-Supervised Classification with Graph Convolutional Networks," arXiv:1609.02907, 2017.
- [19] H. Gao and S. Ji, "Graph U-Nets," arXiv:1905.05178, 2019.
- [20] T. T. Müller, S. Starck, A. Dima, S. Wunderlich, K.-M. Bints, K. Zaripova *et al.*, "A survey on graph construction for geometric deep learning in medicine: Methods and recommendations," *Transact. Mach. Learn. Res.*, 2024.
- [21] H. Zhang, R. Song, L. Wang, L. Zhang, D. Wang, C. Wang *et al.*, "Classification of Brain Disorders in rs-fMRI via Local-to-Global Graph Neural Networks," *IEEE Trans. Med. Imaging*, vol. 42, no. 2, pp. 444–455, 2023.
- [22] X. Song, F. Zhou, A. F. Frangi, J. Cao, X. Xiao, Y. Lei *et al.*, "Multicenter and Multichannel Pooling GCN for Early AD Diagnosis Based on Dual-Modality Fused Brain Network," *IEEE Trans. Med. Imaging*, vol. 42, no. 2, pp. 354–367, 2023.
- [23] C. Ying, T. Cai, S. Luo, S. Zheng, G. Ke, D. He *et al.*, "Do Transformers Really Perform Bad for Graph Representation?" arXiv:2106.05234, 2021.
- [24] Y. Shi, Z. Huang, S. Feng, H. Zhong, W. Wang, and Y. Sun, "Masked Label Prediction: Unified Message Passing Model for Semi-Supervised Classification," arXiv:2009.03509, 2021.
- [25] C. Pellegrini, N. Navab, and A. Kazi, "Unsupervised pre-training of graph transformers on patient population graphs," *Med. Image Anal.*, vol. 89, p. 102895, 2023.
- [26] Z. Guan, J. Yu, Z. Shi, X. Liu, R. Yu, T. Lai *et al.*, "Dynamic graph transformer network via dual-view connectivity for autism spectrum disorder identification," *Comput. Biol. Med.*, vol. 174, p. 108415, 2024.
- [27] A. Di Martino, C.-G. Yan, Q. Li, E. Denio, F. X. Castellanos, K. Alaerts *et al.*, "The autism brain imaging data exchange: Towards a large-scale evaluation of the intrinsic brain architecture in autism," *Mol. Psychiatry*, vol. 19, no. 6, pp. 659–667, 2014.
- [28] P. Bellec, C. Chu, F. Chouinard-Decorte, Y. Benhajali, D. S. Margulies, and R. C. Craddock, "The neuro bureau ADHD-200 preprocessed repository," *NeuroImage*, vol. 144, pp. 275–286, 2017.
- [29] S. Zheng, Z. Zhu, Z. Liu, Z. Guo, Y. Liu, Y. Yang *et al.*, "Multi-Modal Graph Learning for Disease Prediction," *IEEE Trans. Med. Imaging*, vol. 41, no. 9, pp. 2207–2216, 2022.
- [30] Z. Wu, S. Pan, F. Chen, G. Long, C. Zhang, and P. S. Yu, "A Comprehensive Survey on Graph Neural Networks," *IEEE Trans. Neural Netw. Learn. Syst.*, vol. 32, no. 1, pp. 4–24, 2021.
- [31] X. Li, Y. Zhou, N. Dvornek, M. Zhang, S. Gao, J. Zhuang *et al.*, "BrainGNN: Interpretable Brain Graph Neural Network for fMRI Analysis," *Med. Image Anal.*, vol. 74, p. 102233, 2021.
- [32] Y. LeCun, Y. Bengio, and G. Hinton, "Deep learning," *Nature*, vol. 521, no. 7553, pp. 436–444, 2015.
- [33] A. Bessadok, M. A. Mahjoub, and I. Rekik, "Graph Neural Networks in Network Neuroscience," *IEEE Trans. Pattern Anal. Mach. Intell.*, vol. 45, no. 5, pp. 5833–5848, 2023.
- [34] K. Zhao, B. Duka, H. Xie, D. J. Oathes, V. Calhoun, and Y. Zhang, "A dynamic graph convolutional neural network framework reveals new insights into connectome dysfunctions in ADHD," *Neuroimage*, vol. 246, p. 118774, 2022.
- [35] S. Zhang, X. Chen, X. Shen, B. Ren, Z. Yu, H. Yang *et al.*, "A-GCL: Adversarial graph contrastive learning for fMRI analysis to diagnose neurodevelopmental disorders," *Med. Image Anal.*, vol. 90, p. 102932, 2023.
- [36] L. Peng, N. Wang, J. Xu, X. Zhu, and X. Li, "GATE: Graph CCA for Temporal Self-Supervised Learning for Label-Efficient fMRI Analysis," *IEEE Trans. Med. Imaging*, vol. 42, no. 2, pp. 391–402, 2023.
- [37] K. Zaripova, L. Cosmo, A. Kazi, S.-A. Ahmadi, M. M. Bronstein, and N. Navab, "Graph-in-graph (gig): Learning interpretable latent graphs in non-euclidean domain for biological and healthcare applications," *Med. Image Anal.*, vol. 88, p. 102839, 2023.
- [38] Y. Ektefaie, G. Dasoulas, A. Noori, M. Farhat, and M. Zitnik, "Multimodal learning with graphs," *Nat. Mach. Intell.*, vol. 5, no. 4, pp. 340–350, 2023.
- [39] T. Chen, R. Hong, Y. Guo, S. Hao, and B. Hu, "MS²-GNN: Exploring GNN-Based Multimodal Fusion Network for Depression Detection," *IEEE Trans. Cybern.*, vol. 53, no. 12, pp. 7749–7759, 2023.
- [40] Y. Chen, J. Yan, M. Jiang, T. Zhang, Z. Zhao, W. Zhao *et al.*, "Adversarial Learning Based Node-Edge Graph Attention Networks for Autism Spectrum Disorder Identification," *IEEE Trans. Neural Netw. Learning Syst.*, vol. 35, no. 6, pp. 7275–7286, 2024.
- [41] N. Cohen Kalafut, X. Huang, and D. Wang, "Joint variational autoencoders for multimodal imputation and embedding," *Nat. Mach. Intell.*, vol. 5, no. 6, pp. 631–642, 2023.
- [42] D. P. Kingma and M. Welling, "Auto-Encoding Variational Bayes," arXiv:1312.6114, 2022.
- [43] C. J. C. H. Watkins and P. Dayan, "Q-learning," *Mach. Learn.*, vol. 8, no. 3-4, pp. 279–292, 1992.
- [44] A. Vaswani, N. Shazeer, N. Parmar, J. Uszkoreit, L. Jones, A. N. Gomez *et al.*, "Attention is all you need," arXiv:1706.03762, 2017.
- [45] J. Devlin, M.-W. Chang, K. Lee, and K. Toutanova, "BERT: Pre-training of Deep Bidirectional Transformers for Language Understanding," arXiv:1810.04805, 2019.
- [46] L. Cameron, S. Sharad, C. Brian, K. Ranjeet, G. Satrajit, Y. Chaogan *et al.*, "Towards Automated Analysis of Connectomes: The Configurable Pipeline for the Analysis of Connectomes (C-PAC)," *Front. Neuroinform.*, vol. 7, 2013.
- [47] E. T. Rolls, C.-C. Huang, C.-P. Lin, J. Feng, and M. Joliot, "Automated anatomical labelling atlas 3," *NeuroImage*, vol. 206, p. 116189, 2020.
- [48] D. P. Kingma and J. Ba, "Adam: A Method for Stochastic Optimization," arXiv:1412.6980, 2017.
- [49] L. Maaten and G. E. Hinton, "Visualizing Data using t-SNE," *J. Mach. Learn. Res.*, 2008.
- [50] R. V. Marinescu, N. P. Oxtoby, A. L. Young, E. E. Bron, A. W. Toga, M. W. Weiner *et al.*, "Tadpole challenge: prediction of longitudinal evolution in alzheimer's disease," arXiv:1805.03909, 2018.
- [51] Y. Wang, Z. Cui, and Y. Li, "Distribution-consistent modal recovering for incomplete multimodal learning," in *IEEE Int. Conf. Comput. Vis.*, 2023, pp. 22 025–22 034.
- [52] Y. Yang, H. Chen, Z. Chang, Y. Xiang, C. Ye, and T. Ma, "Incomplete learning of multi-modal connectome for brain disorder diagnosis via modal-mixup and deep supervision," in *Proc. Int. Conf. Medical Imaging Deep Learn.* PMLR, 2024, pp. 1006–1018.